American Journal of Astronomy and Astrophysics
2026; 13(1): 1-14
http://www.sciencepublishinggroup.com/j/ajaa
doi: 10.11648/j.ajaa.20261301.11

Revisiting Oxygen Production Pathways: ^{16}O Abundances in 34 Metal-Poor Stars

Dhanjit Talukdar*, Mrinmay Medhi, Apurba Talukdar, Swapnajyoti Sarma, Deva Pratim Mahanta, Abhasri Rajbongshi, Upakul Mahanta, Arup Bharali

Department of Physics, Bhattadev University, Pathsala, India

Email address:

phy.dhanjit@bhattadevuniversity.ac.in (Dhanjit Talukdar), mrinmaymedhi@gmail.com (Mrinmay Medhi),
phy.apurba@bhattadevuniversity.ac.in (Apurba Talukdar), phy.swapnajyoti@bhattadevuniversity.ac.in (Swapnajyoti Sarma),
devapratimmahanta@gmail.com (Deva Pratim Mahanta), rajbongshiabhasri@gmail.com (Abhasri Rajbongshi),
phy.upakul@bhattadevuniversity.ac.in (Upakul Mahanta), phy.arup@bhattadevuniversity.ac.in (Arup Bharali)
*Corresponding author

To cite this article:

Dhanjit Talukdar, Mrinmay Medhi, Apurba Talukdar, Swapnajyoti Sarma, Deva Pratim Mahanta, Abhasri Rajbongshi, Upakul Mahanta, Arup Bharali. (2026). Revisiting Oxygen Production Pathways: ^{16}O Abundances in 34 Metal-Poor Stars. *American Journal of Astronomy and Astrophysics, 13*(1), 1-14. https://doi.org/10.11648/j.ajaa.20261301.11

Received: 10 December 2025 ; **Accepted:** 23 December 2025 ; **Published:** 4 February 2026

Abstract: We investigate how the oxygen isotope ^{16}O is produced in metal-poor stars and whether current nuclear reaction models can explain the oxygen abundances observed in such stars. Our study focuses on proton- and α-capture reactions operating within the Carbon–Oxygen–Fluorine (COF) nuclear reaction chain, using updated reaction rates from recent nuclear physics compilations. Oxygen abundances are calculated under representative stellar conditions and compared with observational measurements for a sample of 34 metal-poor halo and thick-disk stars taken from the literature. The results show that there exists a limited range of stellar temperatures for which the calculated oxygen abundances closely match the observed values. At relatively low temperatures, the oxygen abundance remains nearly constant, indicating that oxygen production and destruction are both inefficient. As the temperature increases beyond about 0.15 GK, oxygen production becomes more effective, leading to an increase in the predicted oxygen abundance. At still higher temperatures, competing nuclear reactions reduce the net amount of oxygen produced, causing the abundance to decline. A statistical comparison between the calculated and observed oxygen abundances shows a strong agreement, with a correlation coefficient of $r = 0.89$. For most stars, the differences between predicted and observed values are small and lie within the uncertainties expected from spectroscopic measurements. The few cases where larger differences are found can be explained by observational uncertainties and stellar mixing processes. Overall, our results indicate that the COF nuclear reaction chain provides a consistent explanation for oxygen production in low-mass, metal-poor stars and plays an important role in shaping the chemical evolution of the early Galaxy.

Keywords: H-burning, Proton-Capture, Metallicity, Open Cluster, Nucleosynthesis, COF Chain

1. Introduction

The chemical composition of stars has long been recognised as a cornerstone of astrophysical research, providing key insights into stellar structure, nucleosynthesis, and the chemical evolution of galaxies. Elemental abundances, derived from high-resolution spectroscopy, act as tracers of the nuclear processes that have shaped the cosmos since the Big Bang. These signatures record the cumulative history of star formation, stellar evolution, and interstellar enrichment, linking microscopic nuclear reactions to macroscopic galactic evolution. The theoretical foundation of nucleosynthesis was first established by Burbidge *et al.* in 1957 [1], who demonstrated how successive nuclear burning stages hydrogen, helium, carbon, and beyond produce the elements observed today. This seminal framework was later refined through detailed treatments of stellar evolution and nuclear reaction networks [2, 4, 27]. Pagel in 2009 [5] provided a comprehensive synthesis of these ideas within the context of galactic chemical evolution, emphasizing how successive stellar generations progressively enrich the interstellar medium with heavier elements.

In the broader galactic context, metallicity plays a pivotal role in tracing stellar ancestry. Friel 1995 [6] and Salaris *et al.* 2002 [7] demonstrated that metal-poor stellar populations ($[Fe/H] < -1.0$) preserve the chemical imprints of the early Galaxy, offering direct evidence of primordial nucleosynthesis and the earliest stellar generations. These early stars, often located in the Galactic halo or ancient globular clusters, formed when the interstellar medium was only slightly enriched by the first supernovae. Their study provides a window into the efficiency of nucleosynthesis under extremely low-metallicity regimes. Globular clusters (GCs) in particular serve as natural laboratories for examining these processes. Being coeval, gravitationally bound stellar systems, they allow abundance studies under well-constrained physical conditions [8, 27]. Most GCs are old (ages $>$ 10 Gyr) and metal-poor ($[Fe/H] \approx -2.5$ to 0.5), reflecting their origin in the early Milky Way. Observational surveys revealed star-to-star variations in light elements such as C, N, O, Na, Mg, and Al patterns inconsistent with standard stellar evolution models and suggestive of internal or self-enrichment processes [9–11]. The existence of multiple stellar populations within GCs is now understood as a signature of complex formation histories, involving feedback from asymptotic giant branch (AGB) stars, fast-rotating massive stars, and possibly interacting binaries. Among light elements, oxygen occupies a central position. As the third most abundant element in the universe, oxygen is a key participant in the CNO cycle, which dominates hydrogen burning in stars more massive than about $1.3\,M_{\odot}$ at core temperatures exceeding 15×10^6 to 20×10^6 K [2, 4]. Observationally, oxygen is typically enhanced in metal-poor stars ($[O/Fe] \approx 0.4 - 0.6$), consistent with its synthesis in massive stars and ejection through Type II supernovae, while iron enrichment continues later via Type Ia supernovae [5, 12, 13].

Empirical studies from the late 20th and early 21st centuries have deepened understanding of oxygen abundance patterns. Tautvaisiene *et al.* 2005 [14] and Carraro *et al.* 2007 [15] observed α-element enhancements and departures from standard galactic chemical evolution trends among open and globular cluster giants, attributing these differences to internal mixing and dredge-up processes. Salaris *et al.* 2002 [7] and Ventura *et al.* 2010 [11] developed theoretical models explaining such oxygen depletions through hot bottom burning and convective mixing in evolved stars. High-resolution spectroscopic studies using the [OI] 630 nm line [12, 16] confirmed oxygen variations and indicated additional influences from rotation, binary interaction, and mass loss [10, 17, 18]. Theoretical progress has complemented these observational findings. During helium-rich advanced burning stages, extended nucleosynthesis pathways operate through sequences of α- and proton-capture reactions at temperatures of 1×10^8 K to 3×10^8 K and densities of about $10^3\,\mathrm{g\,cm^{-3}}$ [4, 11, 19]. These processes govern the formation and destruction of key isotopes, including ^{16}O, and link even-Z and odd-Z element synthesis. Building on this framework Mahanta *et al.* 2023 [20] and Talukdar *et al.* 2025 [21] investigated the extended Ne-Al and CNOF reaction chains, highlighting the effects of temperature, stellar rotation, and convective structure on abundance yields. Recent nuclear measurements refined critical reaction rates such as $^{17}\mathrm{O}(p,\gamma)^{18}\mathrm{F}$, underscoring how small uncertainties in cross sections can alter oxygen production predictions [22]. Finally, metallicity has emerged as a key parameter shaping these abundance anomalies. Observations of low-metallicity clusters reveal enhanced $[\mathrm{Al/Fe}]$ ratios and measurable metallicity spreads among first-generation stars [13, 15]. Type II clusters such as NGC 1261 also display intrinsic $[\mathrm{Fe/H}]$ variations ($\sim$ 0.12 dex), connecting metallicity to the strength of light-element variations and the presence of multiple stellar populations [6, 8].

In this context, the present study investigates the nucleosynthesis of odd-Z proton-capture elements in metal-poor globular cluster stars, focusing particularly on the production and depletion of ^{16}O through α-capture along the COF chain. The modelling incorporates helium-rich, high-temperature environments to simulate extended burning phases and compares the predicted $[O/H]$ values with spectroscopic observations of Galactic clusters [20, 23, 24]. The goal is to assess whether α-capture and proton-capture mechanisms can jointly explain observed [O/Fe], [Na/Fe], and [Al/Fe] correlations and to evaluate the influence of stellar rotation, mixing, and binarity on these abundance trends. By synthesising theoretical and observational perspectives, this study contributes to a unified understanding of light-element variations in metal-poor stellar systems and their implications for Galactic chemical evolution [5, 27].

This paper is structured as follows: *Section 2* details the theoretical framework, the employed nuclear reaction network, the assumed stellar conditions, and the model for rotational-induced mass ejection. *Section 3* employs the methodology for deriving estimated oxygen abundances, describes the observational data sources for the selected open clusters, and presents a detailed comparison between our model predictions and the observed abundances. Finally, *Section 4 and 5* summarises the principal findings and their implications for understanding oxygen nucleosynthesis and stellar chemical enrichment.

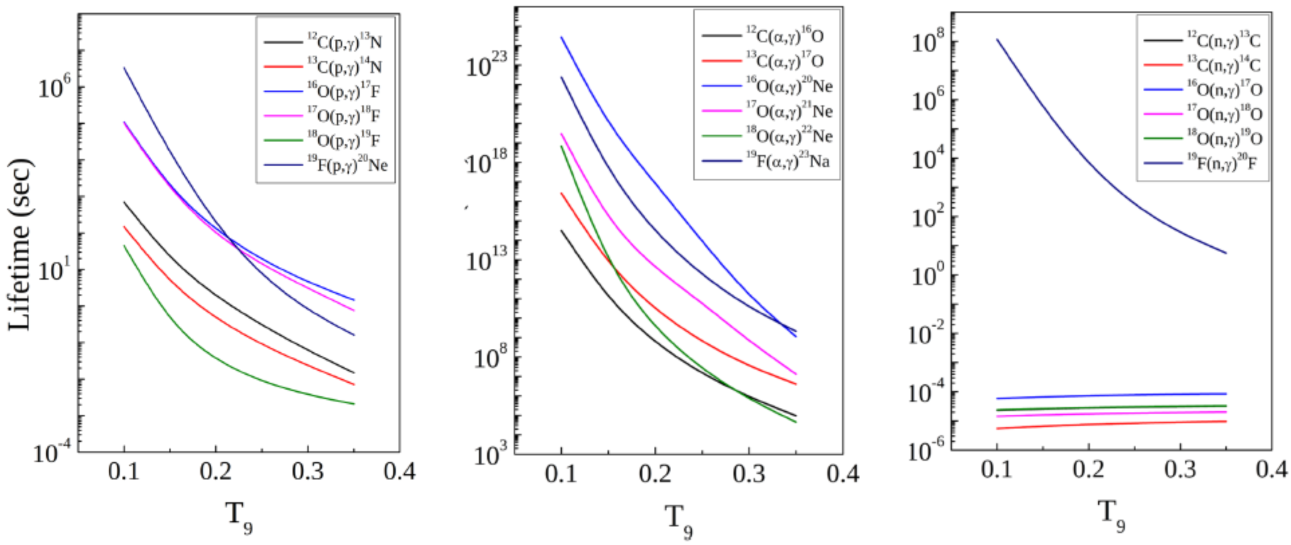

Figure 1. *Temperature-dependent lifetimes of key (p,γ), (α,γ) and (n,γ) reactions involved in the extended COF nuclear reaction network, calculated under representative stellar conditions. Shorter lifetimes indicate dominant reaction pathways within the explored temperature range.*

2. Theoretical Framework and Nuclear Network

The theoretical framework for this study is rooted in the principles of stellar evolution and nucleosynthesis, focusing on the processes that govern the synthesis and distribution of elements within stars, particularly in metal-poor environments characteristic of globular cluster stars. Stellar evolution is primarily driven by successive stages of nuclear burning occurring within the stellar core, where thermonuclear reactions convert lighter elements into heavier ones, releasing energy that counteracts gravitational collapse [25]. These stages are dictated by the star's initial mass, composition, and internal conditions, evolving from hydrogen burning on the main sequence to helium, carbon, oxygen, and beyond in more massive or advanced stars. Temperature emerges as a crucial factor in these stellar processes, determining the onset and efficiency of specific fusion reactions. For instance, hydrogen fusion requires temperatures around 10^7 K, while helium burning initiates at approximately 10^8 K [26, 27]. Density also plays a role, though it is generally less significant in elemental synthesis under conditions of very high temperature and low density, where quantum tunnelling dominates over classical barriers [2, 28].

In constructing stellar models, several simplifying assumptions are typically adopted to make the complex physics tractable. The *standard stellar model* assumes stars to be spherically symmetric, devoid of magnetic fields, without rotation, and experiencing no mass loss from the surface [25, 27]. Spherical symmetry simplifies the equations of stellar structure by reducing them to one-dimensional radial profiles, allowing for the use of the equations of hydrostatic equilibrium, energy transport, and mass continuity [2]. The neglect of magnetic fields disregards their potential influence on convection and mixing processes [29], while the assumption of non-rotation eliminates centrifugal distortion and meridional circulation effects that would otherwise redistribute angular momentum and chemical species [30]. The absence of mass loss further simplifies the modeling, assuming that the total stellar mass remains constant over time, despite stellar winds or ejection events common in evolved stars [31]. Under these assumptions, elements synthesized in the stellar core are transported outward primarily via convection, a process in which hot plasma rises and cooler material sinks, enabling efficient mixing between layers [25]. The boundaries of convective regions are typically determined by the Schwarzschild or Ledoux criteria, which compare temperature and compositional gradients to assess the onset of convective instability [32, 33].

However, real stars often deviate from these idealizations. Rapid rotation, for example, can flatten the star at the poles and induce mixing through shear instabilities or meridional flows, significantly altering surface abundances [29, 30]. Magnetic fields may amplify or suppress turbulence, while mass loss through stellar winds erodes outer layers, exposing processed material [34]. In metal-poor stars, such as those in globular clusters, these effects are amplified due to lower opacities and different convective behaviors. Despite these complexities, the standard model provides a robust baseline for understanding nucleosynthesis, with perturbations added for realism in advanced simulations [31]. Salaris & Cassisi in 2005, [27] emphasize that while spherical symmetry holds for most stars, rotational effects must be included for rapidly rotating objects, where oblateness affects luminosity and temperature distributions [35].

In more evolved stars, particularly those ascending the red giant branch (RGB) or asymptotic giant branch (AGB), specific *dredge-up* events occur that significantly modify surface chemical abundances [36, 37]. Dredge-up refers to the deepening of the convective envelope into regions where nuclear processing has taken place, thereby transporting fusion products to the stellar surface. The *first dredge-up* (FDU) occurs at the base of the RGB when the convective envelope extends inward to reach material previously processed by hydrogen burning after core hydrogen exhaustion. This event leads to observable changes in the surface composition, such as increased helium and altered ratios of light elements like carbon and nitrogen [27, 38]. The *second dredge-up* (SDU) takes place in intermediate-mass stars ($4M_\odot - 8M_\odot$) during the early AGB phase, further enriching the surface with helium and products of hydrogen burning [39, 40]. The *third dredge-up* (TDU), prominent in low- to intermediate-mass AGB stars, follows recurrent helium shell flashes (thermal pulses) and mixes carbon-rich material from the intershell region to the surface, potentially transforming the star into a carbon star [37, 41]. These dredge-up processes play a pivotal role in galactic chemical evolution by releasing nuclearly processed material through stellar winds, enriching the interstellar medium with elements such as carbon, nitrogen, and s-process products [41, 42].

Extra mixing in upper RGB stars could reach the hydrogen-burning shell, triggering further nuclear reactions that contribute to the production of primary elements such as ^{14}N, ^{13}C, ^{16}O and ^{12}C [19]. Observations indicate that standard convective models underpredict surface abundance changes, necessitating additional "extra mixing" mechanisms beyond dredge-up. Proposed processes include thermohaline mixing, driven by inverse μ-gradients from helium-3 burning; rotation-induced shear; or magnetic buoyancy. In low-mass RGB stars, extra mixing depletes lithium and carbon while enhancing nitrogen, as seen in globular cluster stars where CNO anomalies suggest multiple populations. Denissenkov *et al.* 2006 [19] model this in tidally locked binaries, where rotation enhances mixing, leading to primary element production. Such mixing is nearly ubiquitous in low-mass upper RGB stars, with fluid dynamics simulations predicting trends that match observations.

Free neutrons in stellar interiors at $T_9 = 0.1$ K (where T_9 denotes temperature in units of 10^9 K) can be produced via the $^{14}\text{N}(\alpha,\gamma)^{18}\text{F}$ reaction, or other neutron-producing reactions in helium- and carbon-burning stages [2, 35]. At these temperatures, typical of helium-rich advanced burning, the ^{14}N from prior CNO cycling captures an alpha particle, forming ^{18}F, which beta-decays to ^{18}O, potentially leading to further reactions. This chain is part of the pathway to ^{22}Ne production: $^{14}\text{N}(\alpha,\gamma)^{18}\text{F}(\beta^+,\nu)^{18}\text{O}(\alpha,\gamma)^{22}\text{Ne}$, which then serves as a neutron source via $^{22}\text{Ne}(\alpha,n)^{25}\text{Mg}$ during helium burning. Neutron production is vital for s-process nucleosynthesis, where slow neutron captures build heavier elements along the valley of stability [43–45]. At $T_9 = 0.1$ K, the thermal energy of α-particles is considered sufficient to overcome the Coulomb barrier for capture by ^{14}N, initiating the burning process despite the charged-particle repulsion [35, 46].

The proposed COF chain, an extension of the CNO cycle incorporating fluorine, is modelled under helium-rich conditions to explore ^{16}O synthesis [35]. The CNO cycle, dominant in massive stars ($> 1.3M_\odot$), catalytically fuses hydrogen using carbon, nitrogen, and oxygen isotopes, with branches like CN, NO and ON cycles [2, 46]. Under high-temperature conditions, the cycle extends to include fluorine via proton captures, forming the COF chain, where leaks produce neon and sodium. The COF chain begins with neutron capture on ^{12}C, leading to a sequence $^{12}\text{C}(n,\gamma)^{13}\text{C}\ and\ ^{13}\text{C}(\alpha,n)^{16}\text{O}$, followed by proton captures involving ^{16}O to ^{19}F and back [41]. This pathway is relevant in helium-burning stages with residual protons or neutrons, potentially in AGB stars or massive star cores. Wiescher & Langanke in 2010 [47] review such extensions, noting their role in hot bottom burning and proton-ingestion episodes.

Table 1. *Table for Branching Ratio [21].*

T_9	$B_r(^{16}\text{O})$
0.10	131.40
0.15	400.75
0.20	543.41
0.25	496.52

Table 2. *p,γ) lifetimes, τ (in sec), for various nuclear reactions (for ρ = 1 g cm^{-3}).*

Reaction	T_9	$N_A\langle\sigma v\rangle$	τ (Sec)
$^{12}\text{C}(p,\gamma)^{13}\text{N}$	0.10	2.03×10^{-5}	7.04×10^{2}
	0.15	7.46×10^{-4}	1.91×10^{1}
	0.20	7.81×10^{-3}	1.83×10^{0}
	0.25	4.78×10^{-2}	2.99×10^{-1}
	0.30	2.33×10^{-1}	6.13×10^{-2}
	0.35	9.55×10^{-1}	1.50×10^{-2}
$^{13}\text{C}(p,\gamma)^{14}\text{N}$	0.10	9.60×10^{-5}	1.49×10^{2}
	0.15	3.33×10^{-3}	4.29×10^{0}
	0.20	3.18×10^{-2}	4.49×10^{-1}
	0.25	1.63×10^{-1}	8.76×10^{-2}
	0.30	6.10×10^{-1}	2.34×10^{-2}
	0.35	1.98×10^{0}	7.22×10^{-3}
$^{16}\text{O}(p,\gamma)^{17}\text{F}$	0.10	1.30×10^{-7}	1.10×10^{5}
	0.15	8.74×10^{-6}	1.63×10^{3}
	0.20	1.21×10^{-4}	1.18×10^{2}
	0.25	7.77×10^{-4}	1.84×10^{1}
	0.30	3.17×10^{-3}	4.51×10^{0}
	0.35	9.70×10^{-3}	1.47×10^{0}
$^{17}\text{O}(p,\gamma)^{18}\text{F}$	0.10	1.39×10^{-7}	1.03×10^{5}
	0.15	9.65×10^{-6}	1.48×10^{3}
	0.20	1.60×10^{-4}	8.93×10^{1}
	0.25	1.05×10^{-3}	1.36×10^{1}
	0.30	4.61×10^{-3}	3.10×10^{0}
	0.35	1.87×10^{-2}	7.64×10^{-1}
$^{18}\text{O}(p,\gamma)^{19}\text{F}$	0.10	3.17×10^{-4}	4.51×10^{1}
	0.15	4.33×10^{-2}	3.30×10^{-1}
	0.20	4.46×10^{-1}	3.20×10^{-2}
	0.25	1.68×10^{0}	8.50×10^{-3}
	0.30	3.87×10^{0}	3.69×10^{-3}
	0.35	6.80×10^{0}	2.10×10^{-3}

Reaction	T_9	$N_A\langle\sigma v\rangle$	τ **(Sec)**
$^{19}\mathrm{F}(p,\gamma)^{20}\mathrm{Ne}$	0.10	4.31×10^{-9}	3.31×10^{6}
	0.15	9.55×10^{-7}	1.50×10^{4}
	0.20	8.67×10^{-5}	1.65×10^{2}
	0.25	2.14×10^{-3}	6.68×10^{0}
	0.30	1.89×10^{-2}	7.55×10^{-1}
	0.35	8.86×10^{-2}	1.61×10^{-1}

Table 3. *(α,γ) lifetimes, τ (in sec), for various nuclear reactions (for ρ = 1 g cm^{-3}).*

Reaction	T_9	$N_A\langle\sigma v\rangle$	τ **(Sec)**
$^{12}\mathrm{C}(\alpha,\gamma)^{16}\mathrm{O}$	0.10	1.15×10^{-16}	3.11×10^{14}
	0.15	4.18×10^{-13}	8.54×10^{10}
	0.20	7.08×10^{-11}	5.04×10^{8}
	0.25	2.67×10^{-9}	1.34×10^{7}
	0.30	4.19×10^{-8}	8.52×10^{5}
	0.35	3.75×10^{-7}	9.52×10^{4}
$^{13}\mathrm{C}(\alpha,\gamma)^{17}\mathrm{O}$	0.10	1.37×10^{-18}	2.61×10^{16}
	0.15	6.70×10^{-15}	5.33×10^{12}
	0.20	1.40×10^{-12}	2.56×10^{10}
	0.25	6.13×10^{-11}	5.82×10^{8}
	0.30	1.09×10^{-9}	3.28×10^{7}
	0.35	8.78×10^{-9}	4.07×10^{6}
$^{16}\mathrm{O}(\alpha,\gamma)^{20}\mathrm{Ne}$	0.10	1.30×10^{-7}	2.69×10^{24}
	0.15	8.74×10^{-6}	6.98×10^{19}
	0.20	1.21×10^{-4}	8.67×10^{16}
	0.25	7.77×10^{-4}	8.46×10^{13}
	0.30	3.17×10^{-3}	1.25×10^{11}
	0.35	9.70×10^{-3}	1.11×10^{9}
$^{17}\mathrm{O}(\alpha,\gamma)^{21}\mathrm{Ne}$	0.10	1.20×10^{-21}	2.98×10^{19}
	0.15	4.38×10^{-17}	8.15×10^{14}
	0.20	1.02×10^{-14}	3.50×10^{12}
	0.25	5.84×10^{-13}	6.12×10^{10}
	0.30	5.53×10^{-11}	6.46×10^{8}
	0.35	2.70×10^{-9}	1.32×10^{7}
$^{18}\mathrm{O}(\alpha,\gamma)^{22}\mathrm{Ne}$	0.10	5.25×10^{-21}	6.80×10^{18}
	0.15	8.17×10^{-15}	4.37×10^{12}
	0.20	1.35×10^{-11}	2.65×10^{9}
	0.25	1.57×10^{-9}	2.27×10^{7}
	0.30	5.35×10^{-8}	6.68×10^{5}
	0.35	8.01×10^{-7}	4.46×10^{4}
$^{19}\mathrm{F}(\alpha,\gamma)^{23}\mathrm{Na}$	0.10	1.49×10^{-24}	2.40×10^{22}
	0.15	1.24×10^{-19}	2.87×10^{17}
	0.20	1.52×10^{-16}	2.35×10^{14}
	0.25	2.32×10^{-14}	1.54×10^{12}
	0.30	1.06×10^{-12}	3.36×10^{10}
	0.35	1.71×10^{-11}	2.08×10^{9}

Table 4. *(n,γ) lifetimes, τ (in sec), for various nuclear reactions (for ρ = 1 g cm^{-3}).*

Reaction	T_9	$N_A\langle\sigma v\rangle$	τ **(Sec)**
$^{12}\mathrm{C}(n,\gamma)^{13}\mathrm{C}$	0.10	2.18×10^{4}	2.30×10^{-5}
	0.15	1.94×10^{4}	2.58×10^{-5}
	0.20	1.79×10^{4}	2.79×10^{-5}
	0.25	1.69×10^{4}	2.96×10^{-5}
	0.30	1.61×10^{4}	3.10×10^{-5}
	0.35	1.55×10^{4}	3.22×10^{-5}
$^{13}\mathrm{C}(n,\gamma)^{14}\mathrm{C}$	0.10	9.02×10^{4}	5.54×10^{-6}
	0.15	7.52×10^{4}	6.65×10^{-6}
	0.20	6.62×10^{4}	7.56×10^{-6}
	0.25	6.00×10^{4}	8.33×10^{-6}
	0.30	5.55×10^{4}	9.02×10^{-6}
	0.35	5.21×10^{4}	9.59×10^{-6}
$^{16}\mathrm{O}(n,\gamma)^{17}\mathrm{O}$	0.10	8.53×10^{3}	5.86×10^{-5}
	0.15	7.49×10^{3}	6.67×10^{-5}
	0.20	6.85×10^{3}	7.30×10^{-5}
	0.25	6.42×10^{3}	7.79×10^{-5}
	0.30	6.10×10^{3}	8.19×10^{-5}
	0.35	5.89×10^{3}	8.49×10^{-5}
$^{17}\mathrm{O}(n,\gamma)^{18}\mathrm{O}$	0.10	3.47×10^{4}	1.44×10^{-5}
	0.15	3.10×10^{4}	1.61×10^{-5}
	0.20	2.86×10^{4}	1.75×10^{-5}
	0.25	2.69×10^{4}	1.86×10^{-5}
	0.30	2.57×10^{4}	1.95×10^{-5}
	0.35	2.47×10^{4}	2.02×10^{-5}
$^{18}\mathrm{O}(n,\gamma)^{19}\mathrm{O}$	0.10	2.08×10^{4}	2.40×10^{-5}
	0.15	1.88×10^{4}	2.66×10^{-5}
	0.20	1.75×10^{4}	2.87×10^{-5}
	0.25	1.65×10^{4}	3.03×10^{-5}
	0.30	1.58×10^{4}	3.17×10^{-5}
	0.35	1.52×10^{4}	3.28×10^{-5}
$^{19}\mathrm{F}(n,\gamma)^{20}\mathrm{F}$	0.10	4.31×10^{-9}	1.16×10^{8}
	0.15	9.55×10^{-7}	5.24×10^{5}
	0.20	8.67×10^{-5}	5.77×10^{3}
	0.25	2.14×10^{-3}	2.34×10^{2}
	0.30	1.89×10^{-2}	2.64×10^{1}
	0.35	8.86×10^{-2}	5.65×10^{0}

1. $^{12}C(n,\gamma)^{13}C$: This neutron-capture reaction plays a key role in helium-burning and s-process environments. At temperatures around $T_9 \sim 0.1$ K, free neutrons follow Maxwell–Boltzmann distributions with energies sufficient for efficient capture by ^{12}C [35, 43]. The reaction proceeds without significant resonance contributions in the relevant temperature range. Reaction rates are adopted from the NACRE-II compilation and the updated evaluations of Iliadis *et al.* 2010 [4], which show that the capture lifetime remains extremely short ($\sim 10^{-6}$ s) even at low densities.
2. $^{13}C(\alpha,n)^{16}O$: This reaction is the primary neutron source in the s-process occurring in low-mass AGB stars [42, 43]. Its cross-section at astrophysical energies is dominated by the sub-threshold resonance at $E_{\mathrm{cm}} =$ 6.356 MeV in ^{17}O. High-precision measurements by the LUNA collaboration & analyses by Cristallo *et al.* in 2015 [48] and Best *et al.* in 2019 [49] provide updated reaction rates. In the temperature interval $0.1 \leq T_9 \leq 0.2$ K, this reaction efficiently produces both ^{16}O and free neutrons, linking CNO cycling with s-process

nucleosynthesis.

3. $^{16}O(p,\gamma)^{17}F$: This reaction is particularly relevant for $0.06 \leq T_9 \leq 0.1$ K, especially during hot bottom burning in AGB stars [37, 41]. Two resonances at $E_{\rm cm} = 2.50$ and 3.26 MeV are present but make negligible contributions at stellar energies [50]. Reaction rates and uncertainties are taken from Iliadis *et al.* 2010 [4], with an estimated error of about 7% across the astrophysically relevant temperature range $0.01 \leq T_9 \leq 2.5$ K.
4. *Branching on* $^{17}O + p$: After the decay of ^{17}F, proton capture on ^{17}O proceeds through two competing channels:
   (a) $^{17}O(p,\alpha)^{14}N$: This reaction dominates in the temperature range relevant to CNO cycling. Its rate is influenced by a low-energy $E_{\rm cm} = 65$ keV resonance, introducing modest experimental uncertainties. Iliadis *et al.* 2010 [4] report an uncertainty of about 20%, but confirm that this channel overwhelmingly dominates over (p,γ) in the range $T_9 = 0.05 - 0.2$ K, completing the conversion $^{17}O \rightarrow ^{14}N$, and enforcing the cyclic nature of the reaction network.
   (b) $^{17}O(p,\gamma)^{18}F$: This radiative capture channel is significantly weaker. It is controlled by narrow resonances below 400 keV, and updated measurements by Cristallo *et al.* 2015 [48] refine the reaction rate. However, the dominant (p,α) channel ensures that only a small fraction of ^{17}O proceeds to ^{18}F [4].
5. $^{18}O(p,\gamma)^{19}F$: This radiative capture reaction contributes significantly to the production of fluorine in AGB stars. Recent low-energy measurements by the LUNA collaboration [51] extended down to $E_{\rm cm} = 55$ keV, providing improved precision on the reaction cross-section. At temperatures $0.1 \leq T_9 \leq 0.2$ K, the reaction rate is dominated by non-resonant direct capture, following NACRE-II and LUNA results [35, 52].
6. $^{19}F(p,\alpha)^{16}O$: This reaction serves as the destruction channel for fluorine and effectively closes the COF Chain by regenerating ^{16}O. Experimental studies by Pellegriti in 2000 [53] provided the first measurements of the $^{19}F(p,\alpha)^{16}O$ reaction at astrophysical energies.

At temperatures relevant to CNO nuclear processing, this reaction proceeds efficiently, preventing fluorine accumulation and enabling cyclic regeneration of oxygen. Thus, the proposed COF chain proceeds as:

$$
\begin{aligned}
^{12}\mathrm{C} + n &\rightarrow {}^{13}\mathrm{C} + \gamma \\
^{13}\mathrm{C} + {}^{4}\mathrm{He} &\rightarrow {}^{16}\mathrm{O} + n \\
^{16}\mathrm{O} + p &\rightarrow {}^{17}\mathrm{F} + \gamma \\
^{17}\mathrm{F} &\rightarrow {}^{17}\mathrm{O} + e^{+} + \nu_e \\
^{17}\mathrm{O} + p &\rightarrow {}^{14}\mathrm{N} + {}^{4}\mathrm{He} \\
^{17}\mathrm{O} + p &\rightarrow {}^{18}\mathrm{F} + \gamma \\
^{18}\mathrm{F} &\rightarrow {}^{18}\mathrm{O} + e^{+} + \nu_e \\
^{18}\mathrm{O} + p &\rightarrow {}^{19}\mathrm{F} + \gamma \\
^{19}\mathrm{F} + p &\rightarrow {}^{16}\mathrm{O} + {}^{4}\mathrm{He}.
\end{aligned} \tag{1}
$$

The theoretical framework described above provides the basis for modelling the nuclear reaction pathways responsible for oxygen production in stellar interiors. In the following section, this framework is applied to compute oxygen abundances under representative stellar conditions, enabling a direct and quantitative comparison with observed abundances for the selected sample of metal-poor stars.

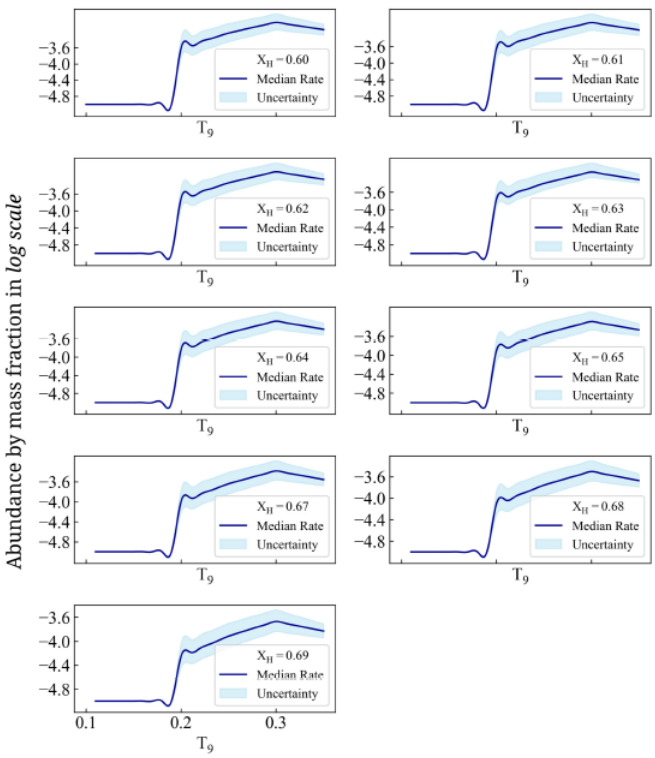

Figure 2. *The estimated mass fraction abundance of* ^{16}O *is plotted as a function of temperature* T_9 *for the hydrogen mass fraction, using the initial condition* $X_{\rm he} = 0.00006$, *across the temperature range* $T_9 = 0.1$ *to* 0.35 K.

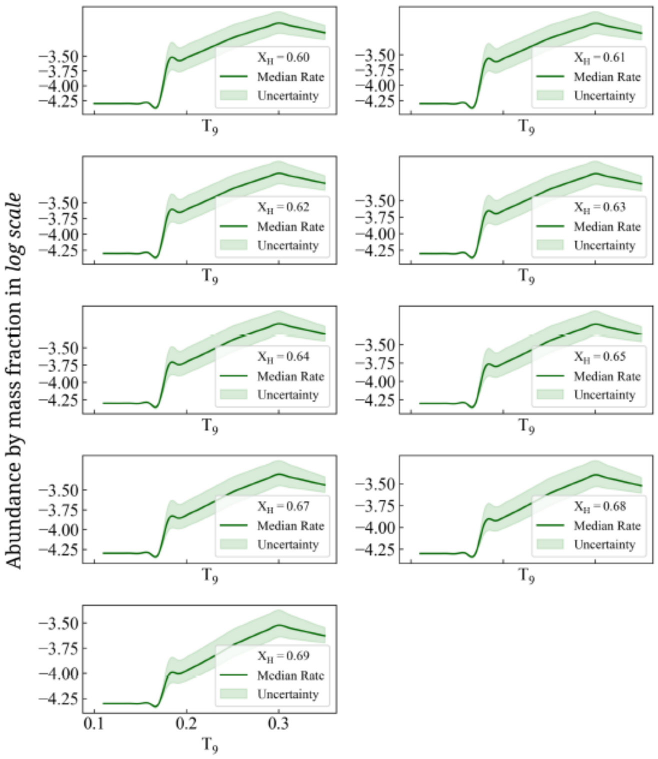

Figure 3. The estimated mass fraction abundance of ^{16}O *is plotted as a function of temperature* T_9 *for the hydrogen mass fraction, using the initial condition* $X_{\rm he} = 0.0003$*, across the temperature range* $T_9 = 0.1$ *to* 0.35 K.

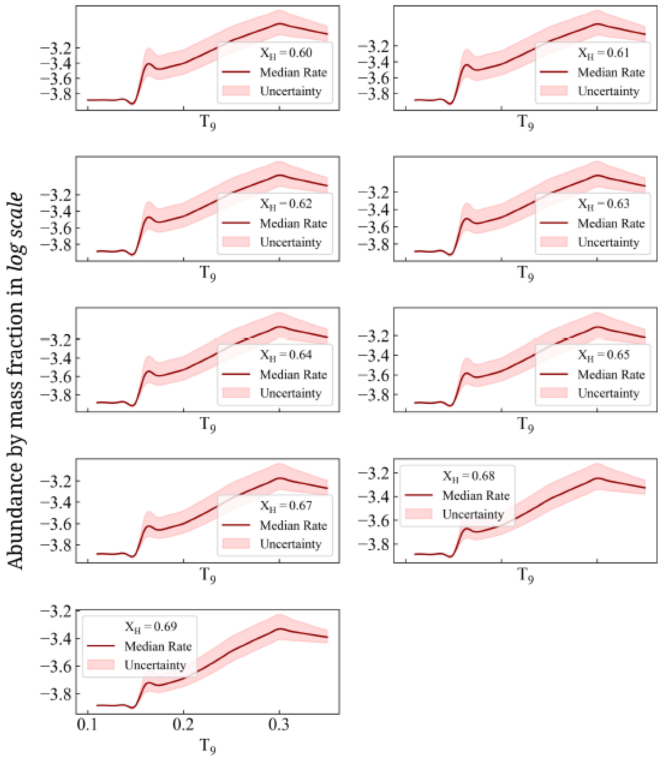

Figure 4. The estimated mass fraction abundance of ^{16}O *is plotted as a function of temperature* T_9 *for the hydrogen mass fraction, using the initial condition* $X_{\rm he} = 0.001$*, across the temperature range* $T_9 = 0.1$ *to* 0.35 K.

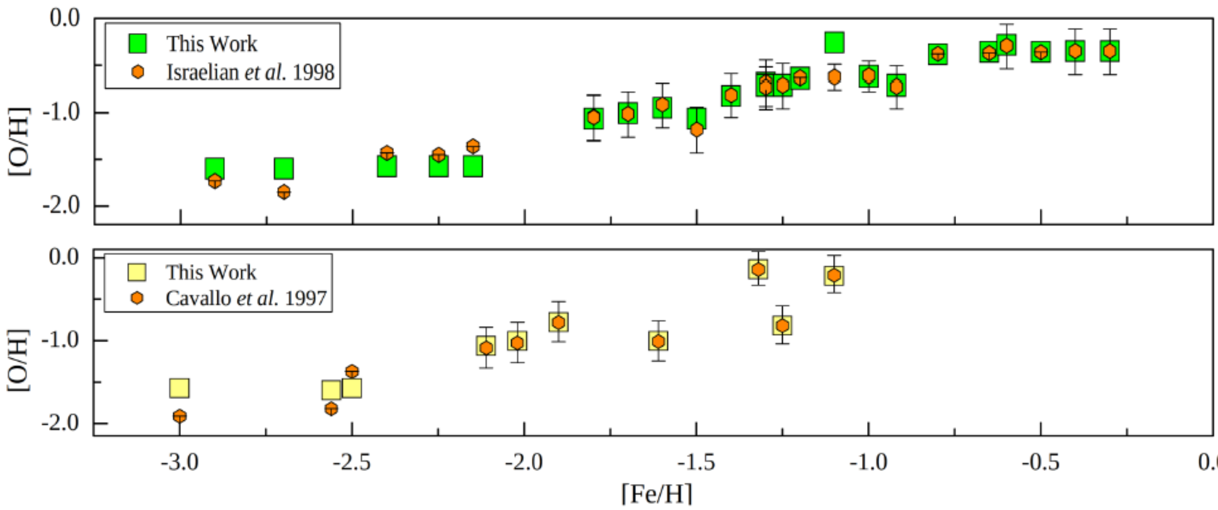

Figure 5. A comparative view of calculated and observed values of abundances of those selected stars of Table 5 is shown. The coloured circles are the values obtained from the literature Israelian et al. 1998 [56] and Cavallo et al. 1997 [57], and the coloured boxes are the values calculated from this work.

3. Methodology and Results

To quantify the chain's efficiency, lifetimes are compared to the number of captures. The rate of a nuclear reaction depends on the density of reactants, their relative velocity, and the likelihood of cross-section [2]. For two species i and j, the rate R is given by equation:

$$R = \sum \frac{1}{1+\delta_{ij}} N_i N_j \langle \sigma v \rangle, \quad (2)$$

where R is the nuclear reaction rate per unit volume, δ_{ij} is the Kronecker delta (equal to unity for $i = j$ and zero otherwise), N_i and N_j are the number densities of the reacting nuclei i and j, and $\langle \sigma v \rangle$ is the thermally averaged reaction rate, obtained by averaging the product of the nuclear cross section σ and the relative velocity v over a Maxwell–Boltzmann distribution. The lifetime against proton capture τ_p at a given density is given by the equation:

$$\tau = \frac{1}{\rho X_p[N_A\langle\sigma v\rangle]}. \tag{3}$$

Here, τ denotes the mean lifetime of a nucleus against proton capture, ρ is the mass density of the stellar plasma, X_p is the hydrogen mass fraction, N_A is Avogadro's number, and $\langle\sigma v\rangle$ represents the thermally averaged proton-capture reaction rate. The Reaction rate constants are taken from NACRE-II and Iliadis *et al.* 2010 [4], who provide Monte Carlo evaluated rates for charged-particle reactions up to $A = 40$, incorporating uncertainties via probability density functions. Similar lifetimes for alpha (τ_α) and neutron (τ_n) captures are computed, allowing comparison of competing processes in the COF chain. Table 2, Table 3 and Table 4 present the computed lifetimes for the (p,γ), (α,γ) and (n,γ) reactions, respectively, for various nuclei under stellar conditions. During the reaction cycle, α-particles are also produced. Although these α particles might initially appear capable of participating in additional (α,γ) reactions potentially introducing new branching points and altering elemental abundance patterns their relevance depends on the corresponding reaction lifetimes. To assess this, the α-capture lifetimes for all stable nuclei were calculated using an expression analogous to equation 3, with X_p replaced by X_{He}. Since reactions with shorter lifetimes dominate under given physical conditions, the most probable pathway is determined by the minimum lifetime among competing processes. As illustrated in figure 1, the (p,γ) reactions exhibit the shortest lifetimes across the temperature range considered, indicating that they are the predominant processes in these stellar environments.

For abundance calculations, Clayton in 1983 [2] formulated a differential equation describing number density evolution, incorporating proton captures, beta decays, or both:

$$\frac{dN_i}{dt} = -N_iN_p < \sigma v >_{p,i} + N_jN_p < \sigma v >_{p,j} \pm\lambda_kN_k, \tag{4}$$

where N_i is the number density of the nucleus i, N_p is the proton number density, and $\langle\sigma v\rangle_{p,i}$ denotes the thermally averaged proton-capture reaction rate for nucleus i. The first term on the right-hand side represents the destruction of nucleus i through proton capture, while the second term accounts for its production from a parent nucleus j via proton capture. The term λ_k is the decay constant associated with β-decay or other relevant decay processes of nucleus k, and the $\pm$ sign indicates whether the decay contributes to the production or destruction of nucleus i.

The time derivative dN_i/dt therefore describes the net change in the abundance of nucleus i due to competing nuclear reactions and decay processes. This framework treats nucleosynthesis as a network of coupled ordinary differential equations (ODEs), where each isotope's abundance changes due to production and destruction terms. Incorporating into the burning cycle for suitable temperatures yields ODEs expressed as functions of hydrogen mass fraction X_H given by equation [2]:

$$\frac{dX_i}{dX_H} = \frac{-R_{p,i}X_i + \frac{A_i}{A_j}R_{p,j}X_j}{-\sum_{A_i}^{A_j}\left(\frac{1}{A_i}R_{p,i}X_i\right)}, \tag{5}$$

where X_i and X_j are the mass fractions of nuclei i and j, respectively, and X_H is the hydrogen mass fraction. The quantities $R_{p,i}$ and $R_{p,j}$ denote the proton-capture reaction rates for nuclei i and j, respectively. The symbols A_i and A_j represent the atomic mass numbers of the corresponding nuclei. The numerator describes the net production and destruction of nucleus i due to proton-capture reactions, with the first term accounting for its depletion and the second term representing its production from nucleus j, scaled by the ratio of atomic masses. The denominator represents the total hydrogen consumption rate summed over the relevant mass range from A_i to A_j, ensuring that the evolution of X_i is expressed relative to changes in the hydrogen abundance. These are solved numerically with initial conditions, often using implicit solvers for stiffness.

The set of four coupled first-order linear differential equations, as detailed in equation 5, is solved numerically to investigate the cycle with variations in the hydrogen mass fraction up to $X_H = 0.60$. This approach allows for the determination of equilibrium mass fraction abundances across different temperatures with appropriate initial conditions. Extremely low metallicity conditions are explicitly considered in the present work, with models extending down to $Z = 0.00006$. Such low heavy-element content leads to reduced opacity, producing more compact and hotter stellar structures with enhanced luminosities. The associated increase in radiation pressure can influence stellar mass retention and rotational evolution, particularly in rapidly rotating main-sequence stars. Previous studies have shown that massive stars with metallicities as low as $Z = 0.0005$ and initial rotational velocities of $\sim 500\ \mathrm{km\,s^{-1}}$ can rapidly reach and sustain near-critical rotation throughout their evolution [9, 60]. These effects are therefore relevant for understanding nucleosynthesis and surface abundance patterns under the extremely low-metallicity conditions explored in this study. To evaluate the equilibrium mass fraction of ^{16}O, the hydrogen mass fraction is fixed at $X_\mathrm{H} = 0.60$, and calculations are performed over the temperature range $T_9 = 0.1$ to 0.35 K. It is further assumed that the total heavy-element mass fraction is uniformly distributed among all heavy nuclei, and the initial abundances therefore follow the universal standard, $X_H + X_{He} + X_{he} = 1$. The heavy-element mass fraction is varied under three cases:

1. $X_\mathrm{he} = (X_{^{12}\mathrm{C}} = X_{^{13}\mathrm{C}} = X_{^{16}\mathrm{O}} = X_{^{17}\mathrm{O}} = X_{^{18}\mathrm{O}} = X_{^{19}\mathrm{F}} = 0.00001) = 0.00006$,
2. $X_\mathrm{he} = (X_{^{12}\mathrm{C}} = X_{^{13}\mathrm{C}} = X_{^{16}\mathrm{O}} = X_{^{17}\mathrm{O}} = X_{^{18}\mathrm{O}} = X_{^{19}\mathrm{F}} = 0.00005) = 0.0003$, and,
3. $X_\mathrm{he} = (X_{^{12}\mathrm{C}} = X_{^{13}\mathrm{C}} = X_{^{16}\mathrm{O}} = X_{^{17}\mathrm{O}} = X_{^{18}\mathrm{O}} = X_{^{19}\mathrm{F}} = 0.00016) = 0.001$.

The observed abundances by the mass fraction of ^{16}O at various hydrogen mass fractions (X_H) are detailed in Figure 2, Figure 3 and Figure 4 across different temperatures (T_9). The abundances of ^{16}O is calculated using:

$$\left[\frac{O}{H}\right] = \left[\frac{O}{Fe}\right] + \left[\frac{Fe}{H}\right], \tag{6}$$

respectively as described by Mahanta *et al.* 2017 [23]. The solar number densities are utilized from the values reported by Lodders in 2003 [55].

The observed abundances for oxygen from Israelian *et al.* 1998 [56], Cavallo *et al.* 1997 [57], are presented in Table 5 for comparison. In Figure 5, the calculated ^{16}O abundances are seen to have a strong correlation with the observed literature values of those selected stars. The calculated abundances at a particular temperature are those for which the difference between observed and calculated abundance is found to be minimal.

Table 5. *The elemental abundances of* ^{16}O *are calculated for different hydrogen mass fractions. All observational data (*$T_{\rm eff}$*,* $\log g$*, [Fe/H], and [O/H]) are taken from Israelian et al. 1998 [56] and Cavallo et al. 1997 [57]. The* Uncertainty *column (*δ*) represents the absolute difference between the observed and calculated oxygen abundances, i.e.,* $\delta = |[\mathrm{O/H}]^o - [\mathrm{O/H}]^a|$. MAD *indicates the Mean Absolute Deviation.*

Star	$\mathbf{T_{eff}}$ **(K)**	**log g**	**[Fe/H]**	**[O/H]^a**	$\mathbf{T_9}$	$\mathbf{X_p}$	**[O/H]^o**	δ	**MAD**
HD 6582	5330 ± 100	4.30 ± 0.15	-0.65	-0.37 ± 0.22	0.19	0.69	-0.36	0.01	
HD 19445	5810 ± 150	4.30 ± 0.10	-2.15	-1.36 ± 0.32	0.10	0.65	-1.57	0.21	
HD 22879	5915 ± 100	4.10 ± 0.15	-0.80	-0.38 ± 0.23	0.17	0.69	-0.38	0.00	
HD 38510	5780 ± 100	3.90 ± 0.10	-0.92	-0.72 ± 0.22	0.26	0.69	-0.71	0.01	
HD 64090	5385 ± 100	4.45 ± 0.10	-1.80	-1.04 ± 0.22	0.20	0.69	-1.06	0.02	
HD 76932	5800 ± 100	3.85 ± 0.10	-1.10	-0.62 ± 0.23	0.35	0.67	-0.26	0.36	
HD 84937	6210 ± 120	4.00 ± 0.10	-2.25	-1.45 ± 0.25	0.10	0.65	-1.57	0.12	
HD 94028	5975 ± 120	4.10 ± 0.10	-1.60	-0.91 ± 0.25	0.22	0.69	-0.95	0.04	
HD 103095	5030 ± 100	4.55 ± 0.35	-1.30	-0.68 ± 0.26	0.20	0.67	-0.69	0.01	
HD 134169	5820 ± 100	3.80 ± 0.15	-1.00	-0.61 ± 0.22	0.33	0.69	-0.62	0.01	
HD 140283	5550 ± 100	3.35 ± 0.10	-2.70	-1.85 ± 0.22	0.19	0.69	-1.60	0.25	
HD 157214	5625 ± 100	3.70 ± 0.15	-0.60	-0.29 ± 0.22	0.22	0.69	-0.28	0.01	
HD 165908	6010 ± 120	4.05 ± 0.15	-0.40	-0.35 ± 0.25	0.20	0.66	-0.35	0.00	
HD 166913	5965 ± 120	3.90 ± 0.20	-1.80	-1.05 ± 0.27	0.20	0.69	-1.06	0.01	
HD 170153	6100 ± 120	4.00 ± 0.20	-0.30	-0.35 ± 0.26	0.20	0.66	-0.35	0.00	
HD 188510	5495 ± 100	4.10 ± 0.10	-1.70	-1.01 ± 0.23	0.21	0.69	-1.01	0.00	
HD 189558	5650 ± 100	3.50 ± 0.10	-1.30	-0.73 ± 0.22	0.26	0.69	-0.71	0.02	
HD 194598	5960 ± 120	4.15 ± 0.10	-1.40	-0.81 ± 0.27	0.24	0.69	-0.82	0.01	
HD 201889	5615 ± 100	3.60 ± 0.15	-1.25	-0.71 ± 0.25	0.22	0.68	-0.71	0.00	
HD 201891	5870 ± 100	4.00 ± 0.10	-1.20	-0.63 ± 0.23	0.13	0.66	-0.64	0.01	
HD 211998	5280 ± 100	3.00 ± 0.20	-1.50	-1.18 ± 0.23	0.20	0.69	-1.06	0.12	
HD 225239	5605 ± 100	3.15 ± 0.20	-0.50	-0.36 ± 0.22	0.19	0.69	-0.36	0.00	
BD +23°3130	5130 ± 150	2.50 ± 0.30	-2.90	-1.73 ± 0.33	0.19	0.69	-1.60	0.13	
BD +37°1458	5260 ± 100	3.00 ± 0.20	-2.40	-1.43 ± 0.27	0.10	0.65	-1.57	0.14	
Star	$T_{\rm eff}$ (K)	log g	[Fe/H]	[O/H]^b	T_9	X_p	[O/H]^o	δ	MAD
BD +17°4708	5890	...	-1.90	-0.78	0.21	0.68	-0.78	0.00	
BD +37°1458	5425	...	-2.11	-1.09	0.20	0.69	-1.06	0.03	
BD 1855550	4580	...	-3.00	-1.91	0.10	0.65	-1.57	0.34	
HD 122563	4650	...	-2.56	-1.82	0.19	0.69	-1.60	0.22	
HD 128279	...	...	-2.50	-1.37	0.10	0.65	-1.57	0.20	
HD 166161	5150	...	-1.32	-0.14	0.29	0.67	-0.14	0.00	
HD 201889	5580	...	-1.10	-0.21	0.25	0.66	-0.22	0.01	
HD 44007	4890	...	-1.61	-1.01	0.21	0.69	-1.01	0.00	
HD 87140	4940	...	-2.02	-1.03	0.21	0.69	-1.01	0.02	
HD 94028	5900	...	-1.25	-0.82	0.24	0.69	-0.82	0.00	
MAD									0.40
Average							-0.88		

^{a} Israelian *et al.* 1998 [56], ^{b} Cavallo *et al.* 1997 [57], ^{o} This work.

4. Results & Analysis

Our analysis reveals that, within the explored temperature–density regime, a relatively narrow interval exists in which the calculated oxygen abundance ratios [O/H] closely reproduce the observed stellar values. At lower temperatures, the oxygen abundance exhibits an almost flat behaviour, indicating that the production of ^{16}O is governed primarily by weakly temperature-dependent and often sub-threshold reaction channels [48]. In this regime, neither significant synthesis nor efficient destruction of ^{16}O occurs, placing these stars in a nuclear "idle zone" with respect to oxygen processing.

As the temperature exceeds $\sim$ 0.15 GK, the Gamow window begins to sample higher reaction cross sections and possible resonant contributions. Under these conditions, production channels such as $^{13}\mathrm{C}(\alpha,n)^{16}\mathrm{O}$ and $^{19}\mathrm{F}(p,\alpha)^{16}\mathrm{O}$ become increasingly efficient and surpass competing destruction pathways, leading to a systematic rise in oxygen abundance. At still higher temperatures, $T_9 \gtrsim 0.3$, destruction channels and leakage toward heavier nuclei grow more rapidly than the dominant production reactions, redirecting the net reaction flow away from the $A = 16$ mass region and causing a decline in the ^{16}O abundance.

The positive correlation observed between increasing helium mass fraction X_{He} and enhanced ^{16}O yields should not be interpreted as a direct consequence of helium enrichment. Rather, it reflects the effect of an increased initial heavy-element (metal) content within the reaction network. Higher metallicity compositions provide a larger reservoir of seed nuclei–particularly carbon and nitrogen isotopes such as ^{12}C and ^{13}C–that actively participate in α-capture pathways, supplying additional "fuel" for the synthesis of α-nuclei including ^{16}O. Metallicity further influences stellar structure through its impact on opacity, convective efficiency, and core-mass evolution, which collectively modulate nuclear burning efficiency and the retention of synthesised oxygen [62]. Consequently, the close agreement between modelled and observed [O/H] values arises naturally from metallicity-driven enhancement of oxygen production rather than from helium abundance effects alone.

Within the stellar sample, a small subset of stars–HD 19445, HD 84937, BD +37° 1458, and HD 128279–exhibit noticeable under-abundances of ^{16}O relative to previously reported literature values. These discrepancies are most plausibly attributed to observational systematics, including non-local thermodynamic equilibrium (NLTE) effects affecting the O I infrared triplet, blending of the forbidden [O I] 6300 Å line with Ni I, telluric contamination, and sensitivity to the adopted stellar atmospheric parameters such as effective temperature T_{eff} and surface gravity $\log g$. Together, these effects provide a coherent explanation for the observed deviations without invoking modifications to the underlying nucleosynthetic framework.

Conversely, stars such as HD 76932, HD 140283, HD 211998, BD +23° 3130, BD 18° 5550, and HD 122563 display clear overabundances of ^{16}O. At temperatures $T_9 > 0.15$, the α-capture reactions $^{12}\mathrm{C}(\alpha,\gamma)^{16}\mathrm{O}$ and $^{13}\mathrm{C}(\alpha,n)^{16}\mathrm{O}$ become highly efficient, while competing destruction channels remain comparatively weak. Many of these stars are observationally classified as α-enhanced [63], and the present reaction network successfully reproduces this expected nucleosynthetic signature.

Overall, Table 5 and Figure 5 demonstrate that the model-predicted [O/H] values closely match the observed oxygen abundances of halo and thick-disk field stars. For the majority of objects, deviations remain within ≤ 0.05 dex, and the overall mean absolute deviation ($\mathrm{MAD} = 0.40$ dex) lies within the scatter typically associated with high-resolution spectroscopic abundance analyses. This level of agreement indicates that α-capture channels involving ^{13}C play a dominant role in shaping the surface oxygen enrichment of low-mass, metal-poor stars.

To quantitatively assess the agreement between the theoretical oxygen abundance estimates $[O/H]^o$ and empirical values $[O/H]^a$ reported in the literature, a statistical comparison was performed for all 34 stars in the sample. The Pearson correlation coefficient is found to be $r = 0.89$, indicating a strong and statistically significant linear relationship between the calculated and observed abundances. This high degree of correlation demonstrates that the theoretical framework reproduces the global abundance trends rather than merely reflecting random scatter, despite the diversity in metallicity, evolutionary stage, and stellar parameters within the sample.

The mean absolute deviation of the observed $[O/H]$ measurements is approximately 0.44 dex, reflecting the combined effects of observational uncertainties, systematic errors, and intrinsic stellar variations. The relatively modest magnitude of this dispersion indicates that most empirical values remain close to the theoretical predictions, supporting the stability of the numerical calculations and the robustness of the adopted reaction network. Deviations between theory and observation are therefore more plausibly attributed to observational systematics and stellar parameter uncertainties than to deficiencies in the nucleosynthetic model itself.

Table 5 summarizes the comparison between predicted and observed ^{16}O abundances, incorporating observational data from Israelian *et al.* (1998) [56] and Cavallo *et al.* (1997) [57]. Figure 5 presents the same comparison as a function of [Fe/H], enabling the abundance behaviour to be examined in relation to metallicity trends. The uncertainties associated with the calculated abundances represent propagated errors arising from differences between the NACRE-II and Iliadis *et al.* (2010) [4] reaction-rate prescriptions. Even under conservative assumptions, these uncertainties remain sufficiently small to preserve consistency between the predicted oxygen abundances and empirical estimates across the full stellar sample.

5. Discussion & Conclusion

In this study, the synthesis of ^{16}O through proton- and α-capture reactions was examined using updated thermonuclear reaction rates from Iliadis *et al.* [4, 35] in combination with the NACRE-II compilation, within the framework of the COF nuclear reaction chain. The resulting oxygen abundances were compared with observational measurements for 24 metal-poor stars reported by Israelian *et al.* (1998) [56] and 10 stars reported by Cavallo *et al.* (1997) [57]. This comparison, illustrated in Figure 5, demonstrates that within a well-defined and relatively narrow temperature interval, the calculated ^{16}O abundances closely reproduce the observed values across a broad metallicity range.

Although the theoretical exploration presented here is focused on intermediate- and high-metal-poor stellar compositions, spanning approximately $-0.3 \gtrsim [\mathrm{Fe/H}] \gtrsim -3.0$, this range provides a stringent test of the physical consistency of proton-capture processes under conditions relevant to halo and thick-disk stars. The overall agreement between model predictions and observations supports the viability of the COF chain as a robust mechanism for oxygen production within this metallicity regime. At the same time, the presence of localised deviations suggests that additional stellar processes may modulate surface oxygen abundances in specific cases.

The transport of proton-capture products to the stellar surface is governed by a combination of internal mixing and dredge-up mechanisms [7, 58]. Denissenkov & Tout [59] demonstrated that meridional circulation and turbulent diffusion, as described by Zahn's rotational mixing formalism, can efficiently convey nucleosynthetically processed material from the radiative region between the hydrogen-burning shell and the base of the convective envelope. Shear instabilities and horizontal turbulence further contribute to the redistribution of chemical species and angular momentum, with rotational mixing playing an increasingly important role at low metallicity [60]. As processed material is transported to the surface, enhanced rotation may trigger mass-loss episodes, releasing enriched material into the surrounding medium. Such mass loss can significantly influence surface abundance patterns: relatively high mass-loss rates tend to suppress abundance anomalies, whereas lower rates allow the development and preservation of surface over-abundances [61].

Despite the simplifying assumptions inherent in the adopted stellar conditions, the close correspondence between calculated and observed ^{16}O abundances indicates that the dominant nuclear pathways responsible for oxygen production are adequately captured by the present reaction network. The success of the model across a wide range of temperatures and compositions suggests that the COF α-capture chain constitutes a major contributor to oxygen synthesis in evolved, low-metallicity stars. Residual discrepancies at the lowest metallicities likely reflect the combined influence of additional astrophysical processes, such as rotation-induced mixing, binary interactions, or pre-enrichment from early supernova events, rather than shortcomings in the nuclear physics itself.

In conclusion, this work demonstrates that the COF nuclear reaction network, operating under helium-rich and metal-poor conditions, can naturally reproduce the observed oxygen abundance patterns in halo and thick-disk stars. The strong agreement between predicted and observed $[\mathrm{O/H}]$ values, together with the model's ability to account for temperature and compositional dependencies, underscores the importance of proton- and α-capture processes in shaping the oxygen content of the early Galaxy. These findings provide meaningful constraints on stellar nucleosynthesis models and offer valuable insights into the chemical evolution of metal-poor stellar populations.

ORCID

0009-0003-1952-2124 (Dhanjit Talukdar)
0000-0002-8154-2009 (Mrinmay Medhi)
0009-0006-2712-4996 (Apurba Talukdar)
0009-0005-4510-7519 (Swapnajyoti Sarma)
0000-0002-2163-3734 (Deva Pratim Mahanta)
0009-0001-2783-2996 (Abhasri Rajbongshi)
0000-0003-0490-2637 (Upakul Mahanta)
0009-0007-2446-5469 (Arup Bharali)

Abbreviations

AGB	Asymptotic Giant Branch
COF	Carbon-Nitrogen-Oxygen-Fluorine
ISM	Interstellar Medium
LUNA	Laboratory for Underground Nuclear Astrophysics
MAD	Mean Absolute Deviation
RGB	Red Giant Branch

Author Contributions

Dhanjit Talukdar: Writing - original draft
Mrinmay Medhi: Data curation, Formal analysis, Validation, Visualisation, Writing – review & editing
Apurba Talukdar: Validation
Swapnajyoti Sarma: Validation
Deva Pratim Mahanta: Validation
Abhasri Rajbongshi: Validation
Upakul Mahanta: Supervision, Writing – review & editing
Arup Bharali: Supervision

Conflicts of Interest

The authors declare no conflicts of interest.

References

[1] E. M. Burbidge, G. R. Burbidge, W. A. Fowler, and F. Hoyle, *Synthesis of the Elements in Stars*, Rev. Mod. Phys., 29, 547–650, 1957. https://doi.org/10.1103/RevModPhys.29.547

[2] D. D. Clayton, *Principles of Stellar Evolution and Nucleosynthesis*, University of Chicago Press, 1983.

[3] M. Salaris and S. Cassisi, *Evolution of Stars and Stellar Populations*, Wiley-VCH, Weinheim, 2005.

[4] C. Iliadis, R. Longland, A. E. Champagne, A. Coc, and R. Fitzgerald, *Charged-particle thermonuclear reaction rates: II. Tables and graphs of reaction rates and probability density functions*, Nuclear Physics A, 841, 31–250, 2010. https://doi.org/10.1016/j.nuclphysa.2010.04.009

[5] B. E. J. Pagel, *Nucleosynthesis and Chemical Evolution of Galaxies*, Cambridge University Press, 2nd edition, 2009.

[6] E. D. Friel, *The Old Open Clusters of the Milky Way*, Annu. Rev. Astron. Astrophys., 33, 381–414, 1995. https://doi.org/10.1146/annurev.aa.33.090195.002121

[7] M. Salaris, S. Cassisi, A. Weiss, *Red Giant Branch Stars: Theoretical Framework*, Publications of the Astronomical Society of the Pacific, 114, 375–402, 2002. https://doi.org/10.1086/342498

[8] S. Randich and L. Magrini, *Light Elements in the Universe*, Front. Astron. Space Sci., 8, 616201, 2021. https://doi.org/10.3389/fspas.2021.616201

[9] T. Decressin, C. Charbonnel, and G. Meynet, *Fast rotating massive stars and the origin of the abundance patterns in globular clusters*, Astron. Astrophys., 464, 1029–1034, 2007. https://doi.org/10.1051/0004-6361:20066013

[10] G. Tautvaisiene, A. Drazdauskas, A. Bragaglia, et al., *CNO abundances and carbon isotope ratios in evolved stars of the open clusters NGC 2324, NGC 2477, and NGC 3960*, Astronomy & Astrophysics, 595, A16, 2016. https://doi.org/10.1051/0004-6361/201629273

[11] P. Ventura and P. Marigo, *Models for asymptotic giant branch stars of low and intermediate mass*, Mon. Not. R. Astron. Soc., 437, 2778–2792, 2010. http://dx.doi.org/10.1111/j.1365-2966.2010.17304.x

[12] A. B. S. Reddy, D. L. Lambert, and G. Gonzalez, *Comprehensive abundance analysis of red giants in the anticentre open clusters NGC 6791, NGC 6819, NGC 7789*, Mon. Not. R. Astron. Soc., 431, 3338–3351, 2013. http://dx.doi.org/10.1093/mnras/stt412

[13] L. Magrini, S. Randich, G. Kordopatis, N. Prantzos, D. Romano, V. Adibekyan, M. Bergemann, K. Cunha, P. de Laverny, A. Recio-Blanco, Š. Mikolaitis, F. Matteucci, V. Silva Aguirre, and O. Snaith, *Open clusters towards the Galactic centre: chemistry and dynamics*, Astron. Astrophys., 523, A11, 2010. http://dx.doi.org/10.1051/0004-6361/201015395

[14] G. Tautvaivsienve, B. Edvardsson, A. Brandenburg, and L. Lindegren, *Chemical composition of evolved stars in the open cluster M 67*, Astron. Astrophys., 360, 499–511, 2005. http://dx.doi.org/10.1051/0004-6361:20041935

[15] G. Carraro, D. Geisler, S. Villanova, P. M. Frinchaboy, and S. R. Majewski, *Old open clusters in the outer Galactic disk*, Astron. Astrophys., 476, 217–227, 2007. http://dx.doi.org/10.1051/0004-6361:20078113

[16] R. Smiljanic, R. Gauderon, P. North, B. Barbuy, C. Charbonnel, and N. Mowlavi, *CNONa and $^{12}C/^{13}C$ in giant stars of 10 open clusters*, Astronomy & Astrophysics, 502, 267, 2009. https://doi.org/10.1051/0004-6361/200811113

[17] A. Bragaglia, P. Sestito, S. Villanova, E. Carretta, S. Randich, M. Tosi, *Old open clusters as key tracers of Galactic chemical evolution. II. Iron and elemental abundances in NGC 2324, NGC 2477, NGC 2660, NGC 3960, and Berkeley 32*, Astronomy & Astrophysics, 480, 79–90, 2008. https://doi.org/10.1051/0004-6361:20077904

[18] P. Sestito, A. Bragaglia, S. Randich, E. Carretta, L. Prisinzano, M. Tosi, *Old open clusters as key tracers of Galactic chemical evolution. I. Fe abundances in NGC 2660, NGC 3960, and Berkeley 32*, Astronomy & Astrophysics, 458, 121–134, 2006. https://doi.org/10.1051/0004-6361:20065175

[19] P. A. Denissenkov, B. Chaboyer, and K. Li, *From Canonical to Enhanced Extra Mixing in Low-Mass Red Giants: Tidally Locked Binaries*, Astrophysical Journal, 641, 1087–1097, 2006. https://doi.org/10.1086/500565

[20] D. P. Mahanta, M. Medhi, and U. Mahanta, *Isotopic abundance estimation of ^{22}Ne and ^{24}Mg using proton capture reaction network in the extended Ne-Al chain*, Journal of Astrophysics and Astronomy, 44, 2, 2023. https://doi.org/10.1007/s12036-023-09987-z

[21] A. Talukdar, A. Rajbongshi, M. Medhi, and U. Mahanta, *Impact of Proton-Capture Reaction Cycles on Isotopic Oxygen (^{16}O) Abundances in Stars from Galactic Open Clusters NGC 2324, NGC 2477, and NGC 3960*, American Journal of Astronomy and Astrophysics, 12, 112, 2025. https://doi.org/10.11648/j.ajaa.20251203.16

[22] LUNA Collaboration, R. M. Gesue, G. F. Ciani, D. Piatti, A. Boeltzig, D. Rapagnani, M. Aliotta, C. Ananna, L. Barbieri, F. Barile, *et al.*, *First direct measurement of the*

64.5 keV resonance strength in the $^{17}O(p,\gamma)^{18}F$ reaction, *Physical Review Letters*, 133, 052701, 2024. https://doi.org/10.1103/PhysRevLett.133.052701

[23] U. Mahanta, A. Goswami, H. Duorah, and K. Duorah, *P-capture reaction cycles in rotating massive stars and their impact on elemental abundances in globular cluster stars: A case study of O, Na and Al*, Res. Astron. Astrophys., 17, 80, 2017. http://dx.doi.org/10.1088/1674-4527/17/8/80

[24] M. Medhi, D. P. Mahanta, and U. Mahanta, *Contribution of proton capture reactions to the abundances of phosphorus and sulfur in FGK stars*, J. Astrophys. Astron., 44, 1, 2023. http://dx.doi.org/10.1007/s12036-023-09913-3

[25] R. Kippenhahn, A. Weigert, and A. Weiss, *Stellar Structure and Evolution*, Astronomy and Astrophysics Library, Springer, 2012. https://doi.org/10.1007/978-3-642-30304-3

[26] G. R. Caughlan and W. A. Fowler, *Thermonuclear reaction rates V*, Atomic Data and Nuclear Data Tables, 40, 283, 1988. https://doi.org/10.1016/0092-640x(88)90009-5

[27] M. Salaris and S. Cassisi, *Evolution of Stars and Stellar Populations*, Wiley, 2005. https://doi.org/10.1002/0470033452

[28] G. J. Mathews, *Nucleosynthesis in Stars: Cauldrons in the Cosmos (Review of Rolfs & Rodney, 1988)*, Science, 241, 1238, 1988. https://doi.org/10.1126/science.241.4870.1238.b

[29] A. Maeder and G. Meynet, *Physics, Formation and Evolution of Rotating Stars*, Springer, 2009.

[30] A. Maeder, *Stellar Evolution with Rotation*, Cambridge University Press, 2000.

[31] N. Smith, *Mass Loss from Stars and the Evolution of Stellar Clusters*, Cambridge University Press, 2014.

[32] M. Schwarzschild, B. Schwarzschild, and W. S. Adams, *On the Pulsation in the Atmosphere of η Aquilae*, The Astrophysical Journal, 108, 207, 1948. https://doi.org/10.1086/145065

[33] P. Ledoux, *Stellar Models with Convection and with Discontinuity of the Mean Molecular Weight*, The Astrophysical Journal, 105, 305, 1947. https://doi.org/10.1086/144905

[34] H. C. Spruit, *Dynamo action by differential rotation in a stably stratified stellar interior*, Astronomy & Astrophysics, 381, 923, 2002. https://doi.org/10.1051/0004-6361:20011465

[35] C. Iliadis, *Nuclear Physics of Stars*, Wiley-VCH, 2015.

[36] I. Iben Jr., *Stellar Evolution. VI. Evolution from the main sequence to the red-giant branch for stars of mass 1 $M_\odot$, 1.25 $M_\odot$, and 1.5 $M_\odot$*, The Astrophysical Journal, 147, 624, 1967. https://doi.org/10.1086/149040

[37] F. Herwig, *Evolution of asymptotic giant branch stars*, Annual Review of Astronomy and Astrophysics, 43, 435, 2005. https://doi.org/10.1146/annurev.astro.43.072103.150600

[38] C. Charbonnel and N. Lagarde, *Thermohaline instability and rotation-induced mixing: I. Low- and intermediate-mass solar metallicity stars up to the end of the AGB*, Astronomy & Astrophysics, 522, A10, 2010. https://doi.org/10.1051/0004-6361/201014432

[39] S. A. Becker and I. Iben Jr., *The asymptotic giant branch evolution of intermediate-mass stars as a function of mass and composition. I. Through the second dredge-up phase*, The Astrophysical Journal, 232, 831, 1979. https://doi.org/10.1086/157345

[40] A. I. Boothroyd and I.-Juliana Sackmann, *The CNO isotopes: deep circulation in red giants and first and second dredge-up*, The Astrophysical Journal, 510, 232, 1999. https://doi.org/10.1086/306546

[41] A. I. Karakas and J. C. Lattanzio, *The Dawes Review 2: Nucleosynthesis and stellar yields of low- and intermediate-mass single stars*, Publications of the Astronomical Society of Australia, 31, 2014. https://doi.org/10.1017/pasa.2014.21

[42] M. Busso, R. Gallino, and G. J. Wasserburg, *Nucleosynthesis in asymptotic giant branch stars: relevance for galactic enrichment and solar system formation*, Annual Review of Astronomy and Astrophysics, 37, 239, 1999. https://doi.org/10.1146/annurev.astro.37.1.239

[43] F. Käppeler, R. Gallino, S. Bisterzo, and W. Aoki, *The s-process: nuclear physics, stellar models, and observations*, Reviews of Modern Physics, 83, 157, 2011. https://doi.org/10.1103/RevModPhys.83.157

[44] M. Jaeger, R. Kunz, A. Mayer, J. W. Hammer, G. Staudt, K. L. Kratz, and B. Pfeiffer, *$^{22}Ne(\alpha,n)^{25}Mg$: The key neutron source in massive stars*, Physical Review Letters, 87, 202501, 2001. https://doi.org/10.1103/PhysRevLett.87.202501

[45] C. Angulo, M. Arnould, M. Rayet, P. Descouvemont, D. Baye, C. Leclercq-Willain, A. Coc, S. Barhoumi, P. Aguer, and C. Rolfs, *et al.*, *A compilation of charged-particle induced thermonuclear reaction rates*, Nuclear Physics A, 656, 3, 1999. https://doi.org/10.1016/S0375-9474(99)00030-5

[46] C. E. Rolfs and W. S. Rodney, *Cauldrons in the Cosmos: Nuclear Astrophysics*, University of Chicago Press, 1988.

[47] M. Wiescher, J. Görres, E. Uberseder, G. Imbriani, and M. Pignatari, *The cold and hot CNO cycles*, Annual Review of Nuclear and Particle Science, 60, 381, 2010. https://doi.org/10.1146/annurev.nucl.012809.104505

[48] S. Cristallo, O. Straniero, L. Piersanti, and D. Gobrecht, *Evolution, nucleosynthesis, and yields of AGB stars at different metallicities. III. Intermediate-mass models, revised low-mass models, and the PH-FRUITY interface*, The Astrophysical Journal Supplement Series, 219, 40, 2015. https://doi.org/10.1088/0067-0049/219/2/40

[49] A. Best, G. F. Ciani, J. Balibrea-Correa, and L. Csedreki, *Direct* $^{13}C(\alpha,n)^{16}O$ *cross section measurement at low energies*, in Nuclei in the Cosmos XV, Springer, 2019, pp. 215-218. https://doi.org/10.1007/978-3-030-13876-9_35

[50] D. R. Tilley, H. R. Weller, and C. M. Cheves, *Energy levels of light nuclei A = 16-17*, Nuclear Physics A, 564, 1, 1993. https://doi.org/10.1016/0375-9474(93)90073-7

[51] G. Gosta, *The SOCIAL project: measurement of the* $^{14}N(p,\gamma)^{15}O$ *cross section*, The European Physical Journal A, 61, 2025. https://doi.org/10.1140/epja/s10050-025-01561-1

[52] Y. Xu, K. Takahashi, S. Goriely, M. Arnould, M. Ohta, and H. Utsunomiya, *NACRE II: an update of the NACRE compilation of charged-particle-induced thermonuclear reaction rates for nuclei with mass number* $A < 16$, Nuclear Physics A, 918, 61, 2013. https://doi.org/10.1016/j.nuclphysa.2013.09.007

[53] M. G. Pellegriti, *Study of the* $^{7}Li(p,\alpha)^{4}He$ *reaction at astrophysical energies through the Trojan Horse Method*, AIP Conference Proceedings, 513, 298, 2000. https://doi.org/10.1063/1.1303385

[54] G. Meynet, *Physics of rotation in stellar models*, in *The Rotation of Sun and Stars*, Springer, 2009, pp. 139-169. https://doi.org/10.1007/978-3-540-87831-5_6

[55] K. Lodders, *Solar system abundances and condensation temperatures of the elements*, The Astrophysical Journal, 591, 1220, 2003. https://doi.org/10.1086/375492

[56] G. Israelian, R. J. Garcia Lopez, and R. Rebolo, *Oxygen abundances in unevolved metal-poor stars from near-ultraviolet OH lines*, The Astrophysical Journal, 507, 805, 1998. https://doi.org/10.1086/306351

[57] R. M. Cavallo, C. A. Pilachowski, and R. Rebolo, *Oxygen abundances in metal-poor subgiant stars from the O I triplet*, Publications of the Astronomical Society of the Pacific, 109, 226, 1997. https://doi.org/10.1086/133878

[58] A. I. Karakas, *Updated stellar yields from asymptotic giant branch models*, Monthly Notices of the Royal Astronomical Society, 403, 1413, 2010. https://doi.org/10.1111/j.1365-2966.2009.16198.x

[59] P. A. Denissenkov and C. A. Tout, *On a physical mechanism for extra mixing in globular cluster red giants*, Monthly Notices of the Royal Astronomical Society, 316, 395, 2000. https://doi.org/10.1046/j.1365-8711.2000.03498.x

[60] G. Meynet, R. Hirschi, S. Ekström, A. Maeder, P. Eggenberger, *Are C-rich ultra iron-poor stars also He-rich?*, Astronomy & Astrophysics, 521, A30, 2010. https://doi.org/10.1051/0004-6361/200913377

[61] M. Vick, G. Michaud, J. Richer, O. Richard, *Population II stars and the Spite plateau Stellar evolution models with mass loss*, Astronomy & Astrophysics, 552, A131, 2013. https://doi.org/10.1051/0004-6361/201220726

[62] L. B. van den Hoek and M. A. T. Groenewegen, *New theoretical yields of intermediate-mass stars*, Astronomy and Astrophysics Supplement Series, 123, 305, 1997. https://doi.org/10.1051/aas:1997162

[63] P. E. Nissen and W. J. Schuster, *Two distinct halo populations in the solar neighborhood: evidence from stellar abundance ratios and kinematics*, Astronomy & Astrophysics, 511, L10, 2010. https://doi.org/10.1051/0004-6361/200913877